JAAS

ROYAL SOCIETY OF CHEMISTRY

CRITICAL REVIEW

View Article Online
View Journal

Cite this: DOI: 10.1039/d5ja00058k

A review of spectral broadening in laser atomic absorption spectroscopy

Erfan Chenshen,[ad] Juntao Tan,[a] Bin Wang,[c] Erlong Jiang,[d] Nan Zhao, *[b]
Shaofeng Zheng,[c] Zeren Luo,[bd] Jiaming Li *[a] and Qingmao Zhang[a]

Received 13th February 2025
Accepted 24th June 2025

DOI: 10.1039/d5ja00058k

rsc.li/jaas

Laser atomic absorption spectroscopy (LAAS) has played a significant role in various fields such as nuclear forensics, chemical detection, medical diagnostics, environmental monitoring, and various industrial sectors, leveraging its unique advantages. However, spectral broadening phenomena significantly impact the accuracy and precision of LAAS measurements. This critical review examines spectral broadening and its implications for LAAS, incorporating recent advances in ultrafast diagnostics, extreme plasma conditions, and data-driven modeling. The convolution of various broadening mechanisms results in the final profile of spectral lines, among which Doppler, Stark, and pressure broadening are the primary sources in LAAS. Though spectral broadenings generally introduce measurement errors, they also provide crucial information about plasma characteristics. The review concludes with future perspectives, highlighting emerging technologies including artificial intelligence and novel suppression strategies that promise to enhance LAAS capabilities beyond current limitations.

1. Introduction

Atomic absorption spectrometry (AAS), also referred to as atomic absorption spectrophotometry, is a critical technique widely applied in both qualitative and quantitative analyses.[1] Traditional AAS methods include flame atomic absorption spectrometry (FAAS),[2–4] graphite furnace atomic absorption spectroscopy (GFAAS) also called electrothermal atomization (ETAAS),[5–8] and chemical vapor generation atomic absorption spectrometry (CVG-AAS).[9,10] While these techniques offer significant advantages in analytical methodologies[11] and are supported by well-established technological infrastructure,[12,13] they are not without limitations. Common drawbacks include vulnerability to interference and constraints in analytical applicability.[14,15]

In recent decades, advancements in laser technology have led to the emergence of laser atomic absorption spectroscopy (LAAS) as a powerful and versatile technique for detection, analysis, and measurement across various fields. LAAS employs lasers as light sources for spectroscopy, measuring changes in laser beam intensity along an optical path or detecting signals such as electric or magnetic field fluctuations caused by the interaction of laser radiation with a target. These measurements provide information on the composition, concentration, and presence of interfering substances in the sample. LAAS incorporates several atomization techniques, including flame atomization, graphite furnace atomization, and laser ablation.

Fig. 1(a) illustrates the principle of LAAS. The red arrows depict the laser ablation process, where a high-energy laser beam strikes the target material to produce plasma. The green arrows represent laser absorption, during which the laser passes through the plasma to measure its absorption characteristics. This process yields information such as plasma

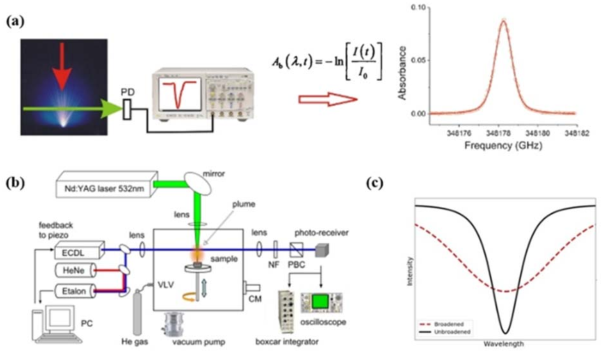

Fig. 1 (a) LAAS system schematic diagram.[37] Copyright (2018), with permission from AIP Publishing. (b) The schematic diagram of tunable diode laser absorption spectroscopy.[38] Copyright (2013), with permission from Springer Nature. (c) An example of broadening spectral line profiles in LAAS.

---

[a] Guangdong Provincial Key Laboratory of Nanophotonic Functional Materials and Devices, School of Optoelectronic Science and Engineering, South China Normal University, Guangzhou, 510006, China. E-mail: jmli@m.scnu.edu.cn; Tel: +86 18594912106

[b] School of Electronics and Information, Guangdong Polytechnic Normal University, Guangzhou, 510665, China. E-mail: zhaonan@gpnu.edu.cn; Tel: +86 18589288025

[c] Guangdong Provincial Key Laboratory of Intelligent Port Security Inspection, Guangzhou, 510510, China

[d] LiSen Optics (Shenzhen) Co., Ltd, Shenzhen, 518000, China

density, temperature, and composition. The Lambert–Beer law applies in LAAS, and the equations in Fig. 1(a) describe the absorption rate calculation at a specific wavelength λ and time t.

Typically, diode lasers are used as light sources in LAAS. The device schematic in Fig. 1(b) demonstrates the stabilization and tuning of an external cavity diode laser (ECDL) *via* feedback to a piezoelectric device controlled by a PC. When the laser passes through plasma generated by Nd:YAG laser ablation, the sample characteristics are analyzed. Data are collected by a photoreceiver and processed using an oscilloscope and a boxcar integrator.

LAAS stands out in high-precision instrumentation systems due to its high sensitivity, rapid response time, and broad detection range. Consequently, it has become a widely favored technique in the academic realm of atomic absorption spectrometry. Moreover, LAAS has found extensive applications in critical scientific domains, including nuclear forensics,[16–18] chemical detection,[19–22] medical diagnostics,[23–25] environmental monitoring[26–29] and various industrial sectors.[30–33]

In LAAS, the evolution of plasma involves various broadening mechanisms arising from characteristic absorption lines of atoms, ions, and molecules, as shown in Fig. 1(c). These mechanisms degrade analytical performance by affecting absorption line widths, positions, and absolute intensities. The solid lines in Fig. 1(c) represent ideal absorption profiles unaffected by broadening, while the dashed line illustrates a broadened absorption profile. As early as 1964, H. R. Griem proposed numerical models and derivation processes for spectral broadening in plasma spectroscopy.[34,35] Over the past several decades, researchers worldwide have continuously refined spectral broadening algorithms, tailoring them for specific applications and leveraging increasingly powerful computational resources to enhance the accuracy of spectral broadening analysis.[36]

In this review, the mechanisms, mathematical models, suppression strategies, and practical applications of spectral broadening in LAAS are systematically examined. Multiple broadening effects often coexist. Their relative dominance depends on experimental conditions such as temperature, pressure, and temporal dynamics. Three primary mechanisms, Stark, Doppler, and pressure broadening, are addressed. Their fundamental principles and recent advancements are elucidated. A bridge between classical atomic spectroscopy and emerging interdisciplinary approaches is provided. A unified framework is established by integrating insights from laser–plasma interactions, ultrafast laser science, and laser materials processing. This framework addresses long-standing challenges in LAAS and offers innovative solutions for high-resolution spectral analysis in extreme plasma environments.

2. Stark broadening

In LAAS applications, Stark broadening often dominates spectral line profiles, particularly in high-density plasma environments. The characteristics and magnitude of this broadening mechanism are strongly influenced by the plasma source used for sample atomization, with electron density being the critical parameter determining Stark broadening intensity across different plasma configurations.

Laser-produced plasma remains the most common atomization source in LAAS, creating conditions where Stark broadening dominates during early plasma evolution due to high electron densities at temperatures of 5000–10000 K. Alternative approaches include arc-jet plasma wind tunnels developed by Kuwahara *et al.*,[39,40] which separate the atomization process from measurement by using a high-temperature upstream section for atomization and a dramatically cooled downstream section for measurements, significantly reducing broadening effects. For specialized applications requiring minimal broadening, low-pressure DC glow discharge systems employed by Jacquet and Pailloux[41] operate at optimized parameters to maintain sufficient sensitivity while minimizing pressure-related broadening effects.

The selection of plasma source fundamentally determines the dominant broadening mechanism, with high electron density environments favoring Stark-dominated profiles. By manipulating temperature, pressure, and geometric configurations of the plasma source as demonstrated by Lebedev *et al.*[42] and Qi *et al.*,[43] researchers can effectively control Stark broadening to achieve the resolution requirements for specific analytical applications, particularly in isotope analysis where minimal line broadening is essential. Among all broadening mechanisms encountered in LAAS, Stark broadening merits detailed examination due to its pronounced impact on spectral resolution under typical high-density plasma conditions. Stark broadening, resulting from collisions between ions and electrons, is often categorized as a unique form of collisional broadening due to its distinct underlying mechanism. Unlike other types of collisional broadening, it originates from the perturbation of atomic energy levels caused by the electric fields of ions or electrons, a phenomenon known as the Stark effect. Broadening induced by a magnetic field, referred to as Zeeman broadening, is another example of field-induced broadening. However, under typical conditions of LAAS, Zeeman broadening is usually negligible.[44] For linear Stark broadening in hydrogen-like elements, the symmetric splitting of energy levels induced by the electric field leads to symmetric broadening of the line width without any displacement. In such instances of linear Stark broadening, the full width at half maximum (FWHM) of the spectral line can be represented by:[45]

$$\Delta\lambda_{1/2}^{s} = [C(n_e, T_e)/n_e]^{2/3} \tag{1}$$

n_e is the electron number density (m^{-3}); T_e is the electron temperature; C is a coefficient depending on n_e and T_e.

In plasma characterization across diverse applications, n_e is a pivotal parameter. A. E. Sherbini *et al.* utilized diode laser atomic absorption spectroscopy (DLAAS) to assess the optical opacity of plasma at the wavelength of the H_α line, demonstrating the feasibility of utilizing Stark broadening under various conditions to evaluate plasma electron density.[46] N. Sadeghi observed that the H_α and H_β lines were sensitive indicators for evaluating the influence of static electric fields, as minimal Stark-induced shifts were detected.[47] N. Konjević *et al.*

analyzed diagnostic procedures for n_e and proposed appropriate recommendations.[48] Certainly, D. M. Surmick *et al.* have proposed semi-empirical formulas under specific conditions through further investigations.[49] The semi-empirical formulas are applicable to plasmas with n_e ranging from 10^{14} to 10^{19} cm^{-3} and temperatures ranging from 1000 to 175 000 K. For instance, the empirical formula for the Stark broadening of the H_α line is as follows.

$$\Delta\lambda_{1/2}^{H_\alpha} = 1.31\left(\frac{n_e}{10^{17}}\right)^{0.64\pm0.03} \tag{2}$$

The Stark effect can exhibit either a linear or quadratic dependence on the electric field. However, with the exception of hydrogen, almost all atoms or ions exhibit quadratic Stark effects. For elements that are not hydrogen like, the interaction is described by:[34,35,50]

$$\Delta\lambda_{1/2}^{s} = 2w\left(\frac{n_e}{10^{16}}\right) + 3.5A\left(\frac{n_e}{10^{16}}\right)^{\frac{1}{4}}\left[1-\frac{4}{3}N_D^{-\frac{1}{3}}\right]w\left(\frac{n_e}{10^{16}}\right) \tag{3}$$

$$\Delta\lambda_{\text{shiff}}^{s} = D\left(\frac{n_e}{10^{16}}\right) + 2A\left(\frac{n_e}{10^{16}}\right)^{\frac{1}{4}}\left[1-\frac{4}{3}N_D^{-\frac{1}{3}}\right]w\left(\frac{n_e}{10^{16}}\right) \tag{4}$$

w is the electron–impact parameter (m); A is the ion broadening parameter; N_D is the number of particles in the Debye sphere; D is the ratio of shift to width (dimensionless). The electron–impact parameter is a significant parameter introduced by H. R. Griem.[34] Subsequent research has continually explored its regularities and systematic trends.[51–55] In eqn (3) and (4), the first term accounts for the broadening and displacement caused by electron collisions, while the second term represents the ion correction factor. Stark broadening induced by electrons typically follows a Lorentzian lineshape, although slight asymmetry can occur.

While Griem's pioneering work in the 1960s established the theoretical framework for Stark broadening analysis, recent studies have exposed critical limitations of classical semi-empirical models in modern LAAS systems. The conventional Griem formalism, relying on assumptions of local thermodynamic equilibrium (LTE) and statistical independence between emitters and perturbers, fails to adequately describe the transient, non-equilibrium conditions inherent to laser-produced plasmas (LPPs).

State-of-the-art spatiotemporally resolved diagnostics reveal that LPPs frequently operate under non-LTE conditions, particularly during early plasma evolution where Stark broadening dominates. Liu *et al.* demonstrated through spatiotemporal diagnostics that electron energy distribution functions in LPPs deviate markedly from Maxwellian distributions, necessitating the use of Druyvesteyn functions for accurate modeling.[56] This non-thermal behavior fundamentally undermines classical Stark broadening tables derived from LTE assumptions, with corrected non-LTE models revealing systematic discrepancies of up to 40% in electron density measurements compared to traditional Griem-based methods.

A critical challenge in LAAS applications involves interpreting Stark broadening parameters from spatially integrated spectra. Thouin *et al.* revealed that unlike emission intensities, which scale linearly with spatial integration, linewidth parameters exhibit nonlinear behavior that defies simple averaging approximations.[57] This finding has profound implications for LAAS measurements, where spatial resolution is often sacrificed for signal intensity, potentially leading to systematic errors in electron density determinations that can exceed 50% in highly inhomogeneous plasmas.

In the initial phases of plasma evolution, when electron number density is elevated, pronounced Stark broadening phenomena are often observed. Harilal *et al.* quantified this phenomenon in ultrafast laser-ablated aluminum plasmas ($t \leq$ 3 μs), showing that absorption line shapes directly encode electron density gradients and plasma inhomogeneity.[58] This effect provides critical insights into plasma electron density diagnostics and spatial inhomogeneity characterization, though it simultaneously complicates the isolation of other broadening mechanisms during these temporal regimes. Complementary observations by N. L. LaHaye *et al.* in laser-produced plasmas confirmed Stark broadening dominance in absorption linewidths, exemplified by the diagnostic utility of the Ca II 315.887 nm transition for precise electron density measurements under high-density conditions, as shown in Fig. 2.[59] Radhakrishna *et al.* then extended these time-resolved approaches by developing a broadband ultraviolet ultrafast laser absorption imaging (UV-ULAI) technique for single shot, high resolution measurements of temperature and CN concentration in HMX flames, leveraging high intensity laser fields that induce Stark shifts to enhance spectral resolution in the measured CN absorbance spectra.[60] Collectively, these breakthroughs highlight spectral broadening analysis as an indispensable tool for resolving ultrafast thermochemical dynamics in LAAS.

During the initial stages of laser-induced plasma evolution, strong Stark broadening significantly influences spectral profiles, hindering the detection of isotope absorption lines. As the plasma expands and cools, the impact of Stark broadening gradually diminishes, resulting in narrower and more distinct spectral features. Early studies, such as those by A. Quentmeier

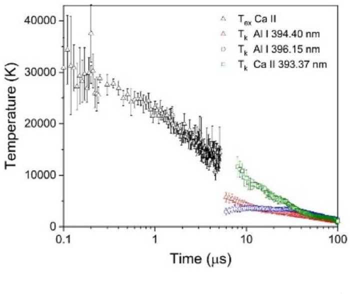

Fig. 2 Excitation and kinetic temperature trends for Ca II and Al I transitions.[59] Copyright (2021), with permission from Elsevier B.V.

et al., observed that during uranium isotope analysis using laser ablation and diode laser atomic absorption spectrometry, the plasma was heavily affected by Stark broadening, making it challenging to detect absorption lines of minor isotopes.[61]

S. S. Harilal *et al.* studied isotopic shifts and hyperfine structures of uranium transitions using tunable laser-induced fluorescence and time-resolved laser absorption spectroscopy in laser ablation plumes.[62] Their results demonstrated that the early evolution of nanosecond LPP is characterized by significant Stark broadening effects, which gradually decrease over time as the plasma expands and cools, as shown by the linewidth evolution in Fig. 3(a).[63] Similarly, Fig. 3(b) illustrates time-resolved absorbance maps, where spectral features are initially dominated by Stark broadening but progressively narrow as the plasma cools and becomes less dense. N. Q. Minesi *et al.* utilized Stark broadening to determine electron number density in partially ionized plasmas.[64] They showed that Stark broadening, caused by charged particle interactions with atomic energy levels, becomes dominant at high ionization levels.

The parameters used to calculate Stark broadening were derived from literature on the broadening of various elements in LAS and atomic spectroscopy databases. The National Institute of Standards and Technology (NIST) maintains a comprehensive database on atomic line broadening, which is crucial for applications in plasma physics and astrophysics. While impact parameters for Stark broadening are widely available for low- and mid-atomic number elements,[65] data for high-atomic number elements remain limited. Consequently, the Stark broadening of low- and mid-atomic number elements can be employed as a diagnostic tool for measuring various physical parameters, rather than being solely regarded as a source of interference.

Stark broadening is prevalent across various applications of LAAS, particularly in laser ablation atomization, where strong electric or magnetic fields are generated during laser ablation. These fields are especially significant in isotope analysis.[37] In isotope analysis, the high sensitivity of LAAS is particularly effective for detecting isotope shifts.[66] Isotope shift refers to the slight relative displacement of atomic energy level centroids among isotopes of the same element, caused by differences in nuclear structure. This phenomenon is observed as a relative shift in the spectral line frequencies of different isotopes in emission or absorption spectra.

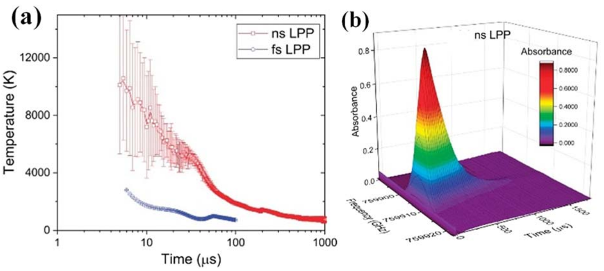

Fig. 3 (a) Linewidth (FWHM) for the Al transition at 394.4 nm and (b) 3D contour maps of absorbance at various frequencies and times.[63] Copyright (2021), with permission from Elsevier B.V.

H. Liu *et al.*, in their study using laser ablation diode laser atomic absorption spectroscopy (LA-DLAAS) to measure solid uranium samples, identified Stark broadening of absorption lines as a significant obstacle to ion detection.[67] Similarly, E. J. Kautz *et al.* examined the effect of Stark broadening on lithium emission spectra, focusing on the 670.8 nm transition, a key spectral line for lithium isotopic analysis.[68] They found that higher pressures increased electron density, resulting in significant Stark broadening and line distortion, which made resolving isotopic shifts challenging. This issue is critical for distinguishing between ^{6}Li and ^{7}Li in isotopic detection applications. M. Burger *et al.* reported measurements of uranium Stark broadening parameters under in a low-pressure environment, with errors falling within an acceptable range of ±45%.[17] G. Hull *et al.* employed combined laser ablation-tuneable diode laser absorption spectroscopy and laser-induced breakdown spectroscopy for the rapid isotope analysis of uranium.[16] The isotope separation results are presented in Fig. 4. When calculating electron density using Stark broadening, the primary source of error originates from uncertainties in the Stark broadening parameters.

They only utilized the first part of eqn (5), which considers only the electron number density by:[69,70]

$$\Delta\lambda_{1/2}^{\mathrm{s}} = 2wn_{\mathrm{e}}10^{-16} \tag{5}$$

where the second part accounting for ion effects was omitted due to negligible errors.[16] Using the same method, researchers analyzed laser-generated lithium plasma and utilized the Stark broadening of lithium emission lines in LIBS spectra to enhance the accuracy of electron density predictions in plasmas generated by laser ablation.[20] M. Miyabe *et al.* have extensively studied LAAS, particularly focusing on lanthanide and actinide elements. They found that Stark broadening and pressure broadening significantly influence spectral resolution and isotopic abundance in the analysis of elements such as uranium (U), plutonium (Pu), and cerium (Ce). To mitigate these effects, researchers frequently adopt low-pressure experimental environments.[71–75] R.G. Wala *et al.* analyzed Stark broadening to estimate electron densities in uranium plasmas. Their findings revealed that the Lorentzian component of spectral lines indicated Stark broadening dominance at early stages, where

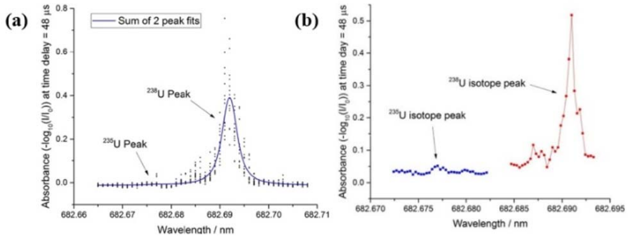

Fig. 4 (a) LA-TDLAS spectrum with a Voigt fit showing ^{238}U at 682.692 nm and ^{235}U at 682.677 nm (masked by noise). (b) Detailed absorption spectrum of uranium isotopes. Each point is the average of 15 laser shots.[16] Copyright (2022), with permission from Elsevier Science B.V.

electron densities were high, gradually decreasing as the plasma cooled. This enabled precise characterization of charge properties in uranium plasmas.[76] Although the impact of Stark broadening has been reduced, Doppler broadening still introduces errors in isotopic abundance estimation.

Research findings emphasize that Stark broadening plays a pivotal role in the evolution of plasma in LAAS, with electron number density serving as a critical parameter for plasma characterization across diverse applications. Researchers employ various LAAS techniques to evaluate electron density. Although semi-empirical formulas have been proposed for specific conditions, their applicability depends on factors such as electron collisions and ion correction factors. Furthermore, the limited availability of Stark broadening data for high-atomic-number elements highlights the need for continued investigation in this area.

3. Doppler broadening

In the early stages of plasma evolution, Stark broadening, caused by collisions with electrons and ions, is the primary contributor to line broadening, often limiting the spectral resolution of LAAS measurements. To address this challenge, researchers typically extend the delay in plasma detection or reduce the pressure in the experimental setup. However, extending the detection delay can reduce spectral intensity, potentially introducing distortion. On the other hand, reducing pressure often shifts the primary broadening mechanism to Doppler broadening, which assumes prominence under low-pressure conditions.[75]

When only the electronic effects of Stark broadening are considered, and the ion correction factor is neglected, Stark broadening is directly proportional to the electron number density. This relationship can be derived from the ideal gas equation:

$$PV = nRT \tag{6}$$

P represents pressure in pascals (Pa), V denotes gas volume in cubic meters (m^3), n stands for the amount of substance of the gas in moles (mol), R denotes the ideal gas constant, also known as the molar gas constant or universal gas constant, with a value of 8.31 in units of joules per mole-kelvin ($\mathrm{J\ mol^{-1}\ K^{-1}}$), and T represents temperature in kelvin (K). In practical applications, when the gas is under high temperature and low-pressure conditions, it can be approximated as an ideal gas. Under these circumstances, the electron number density is directly proportional to the gas pressure. Therefore, conducting experiments in low-pressure environments can reduce Stark broadening, while Doppler broadening typically becomes the dominant mechanism for line broadening.

Assuming photons of a certain frequency are simultaneously radiated, according to the relationship between their velocity and frequency, the Doppler shift in frequency will be:

$$\nu = \nu_0\left(1 + \frac{v}{\mathrm{c}}\right) \tag{7}$$

ν is the observed frequency, ν_0 is the rest frequency, which refers to the transition eigenfrequency of the atoms or molecules, v is the velocity of the emitter towards the observer, and c is the velocity of light ($\mathrm{m \cdot s^{-1}}$). Since the frequency distribution of the radiated photons is proportional to the velocity distribution of the atoms or molecules, eqn (8) can be rewritten as:

$$\frac{n_\mathrm{i}(\nu)}{N_\mathrm{i}}\mathrm{d}\nu = \frac{\mathrm{c}}{v_0\nu_0\sqrt{\pi}}\exp\left\{-\left[\frac{(\nu_0 - \nu_0)\mathrm{c}}{v_0\nu_0}\right]^2\right\}\mathrm{d}\nu \tag{8}$$

v_0 is the most probable velocity. When $\nu = \nu_0$, Doppler spectrum intensity $I_\mathrm{D}(\nu)$ equals the constant term $\frac{\mathrm{c}}{v_0\nu_0\sqrt{\pi}}$ mentioned earlier. Therefore, $I_\mathrm{D}(\nu)$ can be rewritten as an exponential term exp in eqn (9):

$$I_\mathrm{D}(\nu) = I_\mathrm{D}(\nu_0)\exp\left\{-\left[\frac{(\nu_0 - \nu_0)c}{v_0\nu_0}\right]^2\right\} \tag{9}$$

Introducing the half-width at half-maximum $I_\mathrm{D}(\nu') = \frac{1}{2}I_\mathrm{D}(\nu_0)$ as shown in Fig. 5(a). It is evident that there are two solutions ν'_1 and ν'_2. The interval between ν'_1 and ν'_2 represents the Doppler broadening, yielding eqn (10)–(12).

$$\nu'_1 = \nu_0 + \sqrt{\ln 2}\,\nu_0\frac{v_0}{\mathrm{c}} \tag{10}$$

$$\nu'_2 = \nu_0 - \sqrt{\ln 2}\,\nu_0\frac{v_0}{\mathrm{c}} \tag{11}$$

$$\Delta\nu_D = \nu'_1 - \nu'_2 = 2\sqrt{\ln 2}\,\nu_0\frac{v_0}{\mathrm{c}} \tag{12}$$

Doppler broadening is caused by the random motion of moving particles, thus this represents a non-uniform broadening of the transition emission line profiles. As shown in Fig. 5(b), a shift towards shorter wavelengths (blueshift) occurs when the source moves towards the observer, while a shift towards longer wavelengths (redshift) is observed when the source moves away from the observer. From the spectral lines and the linearity, it can be observed that: in a gas particle ensemble characterized by velocities conforming to a random Boltzmann distribution, the spectral lines manifest Gaussian lineshape, and the FWHM is finally as follows:

$$\Delta\lambda^\mathrm{D}_{1/2} = \lambda_0\sqrt{\frac{8k_\mathrm{B}T\ln(2)}{mc^2}} \tag{13}$$

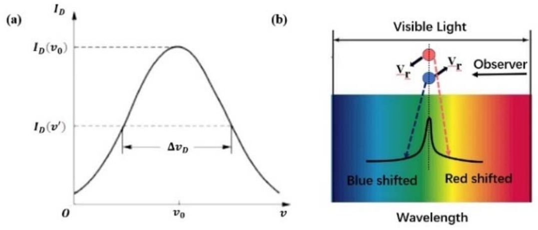

Fig. 5 (a) Doppler broadening spectral line. (b) Wavelength shifts due to Doppler effects.

k_B is the Boltzmann constant ($J \cdot K^{-1}$), and m is the mass of the radiating atom (kg). Can be further simplified by evaluating the constants and substituting the mass m with the atomic or molecular weight $M = m \cdot NA$, where NA is Avogadro's number (mol^{-1}). Therefore, Doppler broadening offers a method for assessing temperature information.

In the realm of LAAS, both macroscopic particles in remote sensing applications[19] and environmental aerosols,[77] as well as microscopic particles such as molecules, atoms, and ions, are subject to the influence of Doppler broadening. However, as this review focuses primarily on AAS, laser absorption spectroscopy techniques involving macroscopic particles are not discussed.

In the measurement of plasma temperature, Harilal *et al.* showed that Doppler broadening became dominant as the plasma cooled and expanded, enabling accurate temperature determination.[58] Harilal *et al.* demonstrated that while Stark broadening dominates in the early stages of nanosecond LPP, Doppler broadening becomes significant at later stages as the plasma cools and expands. This transition is reflected in the narrowing of spectral lines, with Gaussian contributions from Doppler effects becoming more prominent over time.[63] A. Kuwahara *et al.* demonstrated that in the study of aluminum plasma expansion under high-vacuum conditions, Doppler broadening dominated the absorption spectral profiles, leading to observable Doppler splitting.[78] A. Farsy *et al.* demonstrated that in the study of titanium evaporation during electron beam powder bed fusion, Doppler broadening dominated the absorption spectral profiles due to the significant thermal motion of titanium atoms, as shown in Fig. 6(a), where the absorption lines of titanium isotopes were fitted with Gaussian profiles.[79] This approach, illustrated in Fig. 6(b) through the time evolution of laser intensity, enabled precise determination of the vapor temperature.

N. Q. Minesi *et al.* applied Doppler broadening in laser absorption spectroscopy to measure translational temperatures in high-temperature shock-heated gases.[64] They demonstrated that the Gaussian profile's full-width at half-maximum accurately reflects temperature, with results closely matching theoretical predictions. M. C. Phillips *et al.* found that Doppler broadening dominated the spectral line profiles in LPP, enabling the determination of kinetic temperatures by fitting Gaussian linewidths to time-resolved absorption spectra for six uranium transitions.[80] Finally, N. Sadeghi observed that the Doppler broadening of the 1083 nm helium line was used to calculate a gas temperature of 298 K, consistent with theoretical expectations.[47] These findings collectively underscore the critical role of Doppler broadening in accurately characterizing temperature and thermal motion in a variety of high-temperature plasmas and gases.

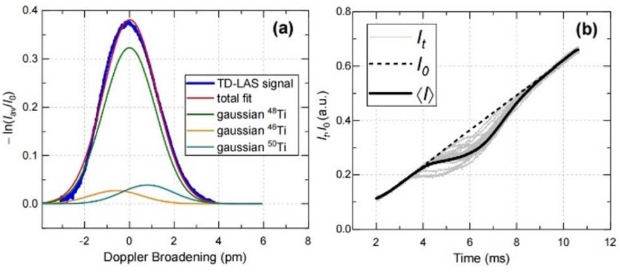

Fig. 6 (a) Absorption profile of titanium isotopes fitted with Gaussian functions, dominated by Doppler broadening. (b) Time evolution of laser intensity before and after passing through titanium vapor, averaged over multiple scans above the melt pool.[79] Copyright (2022), with permission from Elsevier Science B.V.

Doppler broadening is a critical factor in isotope analysis, particularly in laser absorption spectroscopy applications. The following studies highlight its role in various experiments and its influence on isotope analysis across a range of elements and isotopic systems. H. D. Wizemann and K. Niemax applied diode laser atomic absorption spectroscopy (DLAS) to isotopic analysis of Pb in a low-pressure graphite furnace, marking the first instance of isotope dilution calibration in atomic spectrometry. However, Doppler broadening prevented them from directly measuring the concentration of ^{208}Pb.[81] S. Nishiyama *et al.* investigated Doppler broadening of the hydrogen Balmer-α line to estimate the sheath electric field in plasma and successfully determined the translational temperature of hydrogen atoms from the Doppler broadening width.[82]

Building on the impact of pressure-related Stark broadening, E. J. Kautz *et al.* also investigated Doppler broadening and its role in Li isotopic detection. While Stark broadening dominated at higher pressures, Doppler broadening, driven by high plasma temperatures, further widened spectral lines, making isotopic separation more challenging.[68] At lower pressures and cooler plasma conditions, both Stark and Doppler effects were minimized. In extreme plasma conditions, spectral resolution is significantly limited by these broadening mechanisms, presenting major challenges for precise isotopic analysis. L. A. King *et al.* utilized laser ablation-laser atomic absorption spectroscopy (LA-LAAS) for the measurement of Rubidium isotopes.[83] A. Quentmeier *et al.* encountered significant interference from Stark broadening during the early stages of plasma formation in their uranium isotope analysis using laser ablation and diode laser atomic absorption spectroscopy (DLAAS). Furthermore, Doppler broadening also makes it nearly impossible to detect absorption lines of minor isotopes.[61]

To address these limitations, researchers have developed innovative approaches. Kuwahara *et al.* addressed the Doppler broadening challenge by developing a supersonic plasma jet (arc-jet wind tunnel) technique that dramatically reduced translational temperatures from conventional 5000–10000 K to approximately 180 K, improving spectral resolution from the multi-GHz regime to the sub-200 MHz domain and enabling clear differentiation of xenon isotope shifts.[40] Complementarily, Polek *et al.* employed saturated absorption spectroscopy (SAS) to achieve Doppler-free linewidth analysis in uranium LPPs, achieving Lamb-dip spectroscopy with sub-20 MHz resolution in the Doppler-free regime, representing an order of magnitude improvement in spectral resolution compared to conventional absorption methods.[84] These approaches highlight innovative solutions to overcome Doppler broadening effects in extreme plasma environments, opening new possibilities for high-resolution spectroscopy of medium-heavy to heavy elements for isotopic analysis.

To mitigate the effects of Doppler broadening on isotope shifts, isotope analysis experiments are typically conducted under low-pressure conditions. Currently, LAAS has been applied to elements in low-pressure environments such as lead,[81] rubidium,[43,83] uranium,[38,42,61,67,84,85] gadolinium,[77] strontium,[86] xenon,[39–41] calcium[50] and plutonium.[74] For uranium isotopes differing by three neutrons, such as involving nuclear reactions of ^{235}U and ^{238}U, their isotope shifts are merely 25 pm,[87] representing a challenging research subject. Particularly for isotopes that differ by only one neutron, such as ^{239}Pu and ^{240}Pu, their isotope shifts are only around 10 pm,[88,89] which makes differentiation under normal pressure extremely difficult. Consequently, LAAS faces significant challenges in industrial applications.

N. R. Taylor and M. C. Phillips conducted the first measurements of uranium absorption profiles in dry air at 760 Torr using a dual-beam differential absorption method.[90] As shown in Fig. 7, they observed that Doppler broadening dominates at low pressures, while collisional broadening becomes significant at higher pressures due to the increased density of buffer gas molecules. R. G. Wala *et al.* found that Doppler broadening, resulting from the thermal motion of uranium atoms and ions, was essential for determining the kinetic temperature in a laser-produced uranium plasma.[76] By analyzing the Gaussian component of absorption spectra, they tracked the cooling behavior of both neutral uranium and singly-ionized uranium over time.

Doppler broadening has extensive applications beyond isotope analysis, influencing a variety of other fields. Efforts have also been directed toward mitigating the effects of Doppler broadening in LAAS. W. Wei *et al.* successfully reduced Doppler broadening in hyperfine lines by employing saturation absorption spectroscopy. They studied the hyperfine structure of the ^{235}U and ^{238}U isotopes at 861.031 nm and achieved Doppler-free absorption measurements using narrow-band tunable diode lasers and efficient atomic beam generation techniques.[91] In summary, Doppler broadening plays a pivotal role in diverse applications, including flame atomization, plasma temperature diagnostics, and multielement detection. However, its impact introduces systematic errors that can compromise the accuracy of absorption measurements, emphasizing the need for careful optimization of experimental techniques.

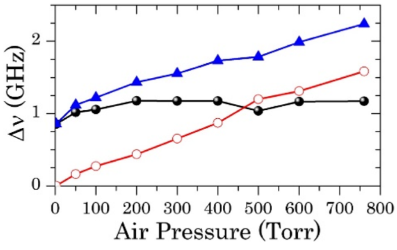

Fig. 7 Pressure dependence of linewidths: Gaussian width (filled circles), Lorentzian width (open circles), and FWHM (triangles). Data obtained from 1.3% uranium filter glass. Uncertainty is negligible.[90] Copyright (2014), with permission from 2014 Optical Society of America.

4. Pressure broadening

At reduced pressures, Doppler broadening typically serves as the primary line broadening mechanism, while at higher pressures, pressure broadening becomes a significant line broadening mechanism.

In the buffer gas, the collisions can induce transitions between different energy levels of the radiator, leading to changes in its spectral characteristics. As shown in Fig. 8(a), when calculating pressure broadening, the sum of the radii d of the two particles is used to obtain the collisional cross section $\sigma = \pi(R_1 + R_2)^2$. Fig. 8(b) illustrates that the volume of interaction is a cylindrical volume with a length equal to the distance traveled by the particle in unit time νt and an area σ. Assuming the colliding particles are of the same type, the mean free path (MFP) can be estimated as shown in eqn (14):

$$s = \frac{\bar{\nu}_s t}{\pi d^2 \bar{\nu}_s t N} = \frac{1}{\pi d^2 N} \tag{14}$$

N is the number of particles per unit volume and $\bar{\nu_s}$ is the distance traveled, which represents the average velocity of atoms undergoing random motion and can be calculated using the Maxwell–Boltzmann distribution. The partial differential with respect to velocity is given by:

$$f(\nu_s)\mathrm{d}\nu_s = \left(\frac{1}{\nu'_s\sqrt{\pi}}\right)^{3/2} 4\pi\nu_s^2 \exp\left[-\left(\frac{\nu_s}{\nu'_s}\right)\right] \times \mathrm{d}\nu_s \tag{15}$$

When this differential equals zero $\frac{\mathrm{d}f(\nu_s)}{\mathrm{d}\nu_s} = 0$, the most probable velocity ν'_s is obtained, as shown in eqn (16):

$$\nu'_s = \sqrt{\frac{2k_B T}{\pi m}} \tag{16}$$

Since all colliding particles are in motion $\bar{\nu_s} = 2\nu'_s$, the average collision time $\tau = \frac{s}{\bar{\nu_s}}$. Based on eqn (14)–(16), the pressure broadening for particles of the same type can be derived by:

$$\Delta\nu_P = \frac{1}{\tau} = N_0\sigma\bar{\nu}_s = 2\sigma\left(\frac{2N_0 P}{\pi m}\right)^{1/2} = 2\sigma P\left(\frac{2}{\pi k_B T m}\right)^{1/2} \tag{17}$$

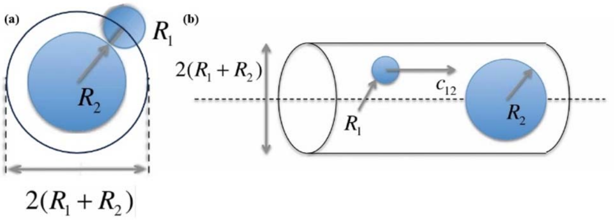

Fig. 8 (a) A simple view of the collisional cross section σ (b) a simple view of the MFP.

The average effect of these collisions results in a spectral line profile characterized by a Lorentzian distribution. When coupled with lifetime broadening, it also modifies the central wavelength of the optical transition. In LAAS experiments, multiple types of particles may collide with each other. The central linewidth and shift induced by pressure can be calculated using the following formula by:[92,93]

$$\Delta\lambda_{1/2}^{\rho} = \sum_i \sigma_i(T_0) P_i \left(\frac{T_0}{T}\right)^{n_i} \tag{18}$$

$$\Delta\lambda_{\text{shift}}^{\rho} = \sum_i \delta_i(T_0) P_i \left(\frac{T_0}{T}\right)^{m_i} \tag{19}$$

$\sigma_i(T_0)$ denotes the pressure broadening coefficient at reference temperature T_0 for the FWHM of the ith perturbing species, with P_i denoting the partial pressure of the perturbing species i. $\delta_i(T_0)$ denotes the shift in line position, measured in nanometers per unit pressure. Its sign indicates either a blue shift or a red shift, as explained earlier. σ_i, δ_i, n_i, and m_i, can be acquired from investigations in high-resolution spectroscopy, where the number density of perturbers and the gas kinetic temperature are controllable parameters, or they can be derived from theoretical computations.[94] Eqn (18) describes the broadening of individual optical transitions of a radiator in a gas mixture composed of atoms, ions, or molecular substances, caused by pressure broadening. Eqn (19) describes the displacement of the center position of the optical transition. In computational and data-driven approaches to LAAS, researchers have developed sophisticated methods to model complex spectral lineshapes and broadening mechanisms. Adowski and Bauman created a comprehensive computational framework for modeling laser absorption in heterogeneous environments that incorporates both pressure broadening and Doppler broadening through Voigt lineshape calculations, enabling more accurate interpretation of LAAS data along arbitrary optical paths with varying temperature and pressure conditions.[95]

This technological advancement, while significantly enhancing temporal and spatial resolution, has concurrently revealed previously unrecognized systematic errors arising from detector nonlinearity and spectral aliasing artifacts.

Machine learning has emerged as a novel and increasingly prevalent methodology in spectral analysis, bridging the gap between theoretical predictions and experimental complexities. The integration of machine learning techniques into spectral broadening analysis represents a paradigm shift from purely theoretical models to hybrid approaches combining physical principles with data-driven optimization. Wang demonstrated that neural network-based algorithms can effectively deconvolve complex line profiles influenced by overlapping broadening mechanisms, achieving superior accuracy compared to conventional least-squares fitting methods.[96] These approaches, however, raise critical questions regarding the physical interpretability of results and potential overfitting risks under specific experimental conditions. Such computational advances substantially enhance our capability to extract precise compositional and thermodynamic information from absorption spectra despite intricate broadening effects. These advancements are particularly critical for resolving subtle pressure broadening phenomena, such as van der Waals interactions in multi-component systems.

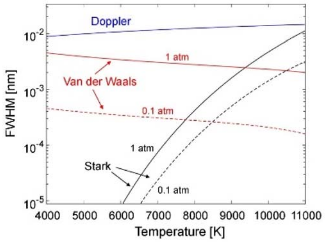

Fig. 9 Calculated broadenings in O2 : Ar mixtures at equilibrium.[64] Copyright (2023), with 2023 Optica Publishing Group.

van der Waals broadening, a specific form of pressure broadening, arises from non-resonant collisions between neutral particles and atoms or ions. It is primarily observed in low-temperature and high-pressure environments, where interactions between neutral particles dominate. In studies of pressure broadening effects, Harilal *et al.* demonstrated that the Lorentzian linewidth of aluminum transitions increases linearly with background pressure. This relationship emphasizes the role of van der Waals interactions in plume confinement and provides precise pressure broadening coefficients for various experimental conditions.[58] N. Q. Minesi *et al.* further analyzed van der Waals broadening, which arises from non-resonant collisions between neutral particles and atomic oxygen.[64] van der Waals broadening significantly contributes to the Lorentzian component at lower temperatures and higher pressures but diminishes rapidly at higher temperatures due to the reduced density of neutral particles (Fig. 9).

During the early stages of LAAS development, researchers employed conventional graphite furnace atomizers[97] and explored LAAS techniques under flame atomization conditions,[98] leading to the first significant improvements in detection limits for LAAS. Both approaches accounted for the influence of pressure broadening. P. Ljung and O. Axner utilized wavelength-modulation laser diode absorption spectrometry in graphite furnaces (WM-LDAS-GF) to detect low concentrations of rubidium.

As LAAS has become increasingly employed in isotope analysis, pressure broadening continues to play a role. However, since most experiments are conducted under low-pressure conditions to mitigate its effects, pressure broadening generally does not emerge as a predominant source of error in isotope analysis. N. R. Taylor *et al.* conducted pioneering measurements of uranium absorption profiles in dry air at 760 Torr using a dual-beam differential absorption method. They found that Doppler broadening dominates line broadening at low pressures, while increasing pressure results in a rise in buffer gas molecules, leading to a corresponding increase in pressure broadening. Addressing these challenges remains a focus for future research.[90] Similarly, H. D. Wizemann and K. Niemax applied DLAS to isotopic analysis of multiple elements in a low-pressure graphite furnace.[98–101] In their measurements of lithium isotopes, they encountered increased uncertainty due to the absence of accurate broadening parameters. When analyzing lead isotopes, Doppler broadening hindered the direct determination of ^{208}Pb concentration, with pressure broadening remaining a key focus.[81]

In recent advances of time-resolved LAAS, ultrafast laser sources have enabled precise characterization of transient species and thermodynamic parameters in high-temperature environments. For instance, Harilal *et al.* employed time-resolved tunable laser absorption spectroscopy to measure Doppler and pressure broadening of the Al I 394.4 nm resonance line in ultrafast LPP, allowing extraction of the temporal evolution of kinetic temperatures and the pressure-broadening coefficient of aluminum.[58] Similarly, Radhakrishna *et al.* developed a broadband UV-ULAI technique for single-shot, high-resolution measurements of temperature and CN concentration in HMX flames, where Voigt lineshapes incorporating both Doppler and collisional broadening were used to fit the measured CN absorbance spectra.[60]

In gas sensing technologies, pressure broadening also plays a critical role in analysis. Most studies focus on macroscopic particles, but some researchers utilize diode laser absorption sensors[102] for atomic combustion diagnostics. T. N. Anderson *et al.* employed diode laser absorption sensors to measure the absorption spectra of atomic mercury, investigating the broadening effects of gases such as air and nitrogen due to collisions with mercury.[103] N. Sadeghi found that under atmospheric pressure, pressure broadening is the dominant mechanism, with resonance broadening impacting singlet states and van der Waals forces influencing triplet states.[47] For the 1083 nm helium line, the Lorentzian width confirmed that line broadening is primarily due to van der Waals interactions and pressure effects. In conclusion, pressure broadening significantly contributes to the understanding of gas-phase interactions and plays a vital role in advancing technologies for isotope analysis, gas sensing, and atomic diagnostics. Its study provides valuable insights into both fundamental physical processes and practical applications, underscoring the importance of continued research in this field.

5. Other broadenings

In the early stages of atomic, ionic, and plasma evolution in LAAS, the system exists in a high-temperature and high-density state. Under these conditions, Doppler broadening, Stark broadening, and pressure broadening are the primary mechanisms responsible for spectral line broadening, while other broadening mechanisms can generally be neglected in experimental settings. The following section presents an overview of the principles and formulae used to calculate additional broadening mechanisms involved in LAAS.

5.1 Natural broadening

In the absence of external influences, excited particles spontaneously transition to lower energy states. As shown in Fig. 10(a), during the process of spontaneous emission, the energy of the system continuously decays, and the harmonic oscillation of the electric dipole's positive and negative centers ceases, resulting in a finite spectral line width known as natural broadening. Natural broadening arises from the finite lifetime of atoms in energy levels, which is caused by inherent spontaneous radiative transitions of each atom. As illustrated in Fig. 10(b), when the positive and negative centers of the electric dipole oscillate harmonically at a frequency ν_0 and with a displacement d, the particles emit electromagnetic waves at the same frequency ν_0. The time-dependent variation of the electromagnetic field generated by these spontaneously emitting particles can be expressed as follows:

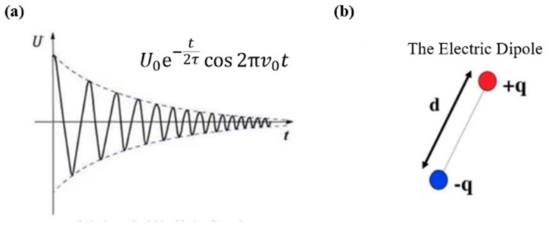

Fig. 10 (a) The damped motion of the electric dipole radiation field. (b) An electric dipole consists of two equal and opposite charges (q and $-q$) separated a distance d.

$$U = U_0 e^{-\frac{t}{2\tau}} \cos 2\pi \nu_0 t \tag{20}$$

$\frac{1}{2\tau}$ is the damping coefficient. The Fourier transform yields eqn (21).

$$\mu(\nu) = \int_{-\infty}^{\infty} U(t)^{e^{-i2\pi\nu t}} \mathrm{d}t \tag{21}$$

When $t < 0$, it can be written as:

$$\mu(\nu) = \int_{-\infty}^{\infty} U(t_0) e^{-\frac{t}{2\tau}} e^{-i2\pi(\nu-\nu_0)t} \mathrm{d}t \tag{22}$$

Therefore, the monochromatic radiation intensity of spontaneous emission can be derived as

$$I(\nu) = \frac{{U_0}^2}{4\pi^2(\nu-\nu_0) + \left(\frac{1}{2\tau}\right)^2} \tag{23}$$

According to the definition of the line profile function, eqn (24), the line profile function for natural broadening can be obtained and its width is characterized by the Lorentzian function eqn (25):

$$f_{\mathrm{N}}(\nu) = \frac{\frac{1}{\tau_{\mathrm{N}}}}{4\pi^2(\nu-\nu_0) + \left(\frac{1}{2\tau_{\mathrm{N}}}\right)^2} \tag{24}$$

$$f_{\mathrm{N}}(v)=\frac{\dfrac{\Delta v_{\mathrm{N}}}{2\pi}}{(v-v_0)^2+\left(\dfrac{\Delta v_{\mathrm{N}}}{2}\right)^2} \quad (25)$$

In eqn (25), v represents the frequency of the spectral line, v_0 denotes the central frequency of the spectral line, and $\Delta v_{\mathrm{N}}=\dfrac{1}{2\pi\tau_{\mathrm{N}}}$ represents the natural broadening of the spectral line.

The average lifetime of the excited-state atoms is approximately 10^{-8} (s). According to eqn (25), Δv_{N} is approximately 10^7 (s^{-1}). The natural broadening of the spectral line is estimated to be on the order of 10^{-5} (nm). Compared to the broadening caused by other factors, which is on the order of 10^{-4} to 10^{-3} (nm), the natural linewidth can be considered negligible.

While natural broadening is generally negligible in most LAAS applications, it becomes a critical limiting factor under specific experimental conditions that demand ultrahigh spectroscopic precision. In ultrahigh-resolution spectroscopy applications, particularly when experimental resolution approaches the natural linewidth limit ($<10^{-5}$ nm), natural broadening can determine the ultimate achievable precision in atomic and molecular systems. This limitation becomes particularly relevant in precision isotope analysis, where natural broadening may constrain the ultimate resolution for closely spaced isotope lines, as demonstrated in high-precision measurements of neodymium isotopes and other heavy elements using ultra-sensitive mass spectrometry techniques.[104]

Notably, precision studies of highly charged ions reveal extreme deviations from ground-state lifetime scaling. In Te-like ions (*e.g.*, Xe^{2+}, Ce^{6+}), the metastable $^1\mathrm{S}_0$ state decays exclusively *via* magnetic dipole (M1) and electric quadrupole (E2) transitions due to strict angular momentum selection rules ($\Delta J=0, \pm1$ for M1; $\Delta J=0, \pm1, \pm2$ for E2). Multi-configuration Dirac–Hartree–Fock calculations predict radiative lifetimes spanning 4.44 ms (Xe^{2+}) to 0.58 ms (Ce^{6+}).[105] Such dramatically extended radiative lifetimes, compared to typical nanosecond-scale excited-state lifetimes, make natural broadening considerations essential for accurate spectroscopic interpretation in precision atomic spectroscopy applications. Orders of magnitude longer than typical ns-scale dipole-allowed transitions. These prolonged lifetimes produce natural linewidths below 100 Hz, necessitating rigorous compensation in precision spectroscopy applications such as quantum logic clock transitions.[106]

5.2 Instrument broadening

While Doppler broadening represents a fundamental physical limit arising from thermal motion of atoms and molecules, the practical resolution achievable in LAAS measurements is often constrained by instrumental limitations that become dominant under specific experimental conditions. This transition from physics-limited to instrument-limited resolution is particularly evident when experimental parameters are optimized to minimize thermal broadening effects.

Spectral resolution in LAAS is fundamentally constrained by instrumental broadening, which is caused by the inherent limitations of optical components. Systematic distortions are introduced by spectrometers and monochromators through grating diffraction limits and finite detector pixel size. The magnitude of these composite artifacts varies with optical configuration. In Lipert's sub-Doppler barium spectrometry experiments, instrumental broadening was identified as the dominant contributor (15 MHz FWHM) under low-pressure conditions (<1 Torr), when collisional broadening was suppressed.[103]

In sub-Doppler regimes where Doppler broadening is suppressed below 10 MHz, power broadening and laser linewidth effects dominate the ultimate resolution limits. Power broadening arises from the nonlinear interaction between high-intensity laser fields (typically >1 MW cm^{-2}) and atomic transitions, inducing Stark shifts that scale with the square root of laser intensity.[50] This effect becomes particularly pronounced in precision spectroscopic applications where high laser intensities are employed to enhance signal-to-noise ratios.

State-of-the-art external-cavity diode lasers have significantly surpassed the 100 kHz barrier, with commercial systems now routinely achieving 50 kHz linewidths and research systems demonstrating sub-kHz performance. Recent advances in frequency stabilization techniques have further enhanced these capabilities, as exemplified by rubidium atomic modulation transfer spectroscopy systems achieving laser linewidths of approximately 65.4 kHz and exhibiting a frequency stability of 4.886×10^{-12} for an averaging time of 32 seconds.[107] These developments represent a critical milestone for high-resolution LAAS applications, where laser frequency stability directly impacts isotopic ratio measurement precision.

The impact of laser linewidth on LAAS performance extends beyond simple spectral resolution considerations. In isotope ratio measurements, where spectral shifts of 0.01–1 GHz must be resolved with high precision, laser frequency jitter and drift can introduce systematic errors that propagate through the entire measurement chain. Modern frequency-stabilized systems employing atomic references provide the long-term stability necessary for extended measurement campaigns, with frequency drifts maintained below 0.2 pm over 25 hour periods.[107]

Furthermore, the availability of narrow-linewidth lasers has enabled new operational regimes in LAAS, particularly in Doppler-free configurations where the intrinsic atomic linewidth (typically 6–10 MHz for allowed transitions) becomes the limiting factor rather than laser characteristics. This transition from laser-limited to physics-limited resolution represents a fundamental shift in LAAS capabilities, opening possibilities for ultrahigh-resolution isotopic analysis previously unattainable with broader linewidth sources.

As experimental instruments[108] and methods[109] for LAAS continue to improve, instrumental broadening has gradually decreased and now typically remains within a small range, rarely serving as the primary broadening factor in LAAS. Beyond the mechanisms mentioned above, when using laser ablation (LA) to generate laser-induced plasma (LIP), emission light may be absorbed as it passes through the plasma. This occurs due to a significant population of atoms in lower energy states within the non-uniform plasma, a phenomenon known as self-absorption.[110] Self-absorption causes the spectral line profile to become distorted and broadened.

5.3 Future developments

A transformative era is heralded by the rapid evolution of LAAS technology. Current limitations are expected to be transcended by the convergence of theoretical advances, instrumental innovations, and computational breakthroughs. Experimental capabilities are approaching fundamental physical limits. Emerging technologies are reshaping the traditional hierarchy of broadening mechanisms. Stark, Doppler, and pressure effects have previously dominated. Unprecedented spectroscopic precision is now being enabled.

Perhaps the most significant theoretical paradigm shift in modern LAAS is the transition from LTE to non-LTE modeling. Traditional semi-empirical models have served the spectroscopy community for decades. These models are now inadequate for complex transient phenomena in laser-produced plasmas. Future theoretical frameworks must incorporate time-dependent collisional-radiative models. Such models must capture plasma evolution from initial ablation through thermalization. This requirement is especially critical during early phases when electron densities exceed 10^{18} cm^{-3} and Stark broadening dominates spectral profiles. A promising pathway involves integrating machine learning with first-principles quantum mechanical calculations. This approach could generate comprehensive broadening parameters for high-atomic-number elements. At present, data scarcity for elements beyond $Z = 50$ limits isotopic analysis of actinides and lanthanides.

Instrumental capabilities are advancing at an unprecedented pace. Laser linewidth improvements have yielded a quantum leap in achievable resolution. Linewidths have progressed from MHz levels in early external-cavity diode lasers to sub-Hz in current systems. Modern frequency-stabilized lasers with linewidths below 65 kHz and frequency stability of 4.886×10^{-12} at an averaging time of 32 s have been developed. Previously undetectable isotopic shifts and hyperfine structures can now be resolved. The technological revolution extends beyond linewidth reduction. Spatiotemporal super-resolution techniques now combine femtosecond temporal resolution with sub-micrometer spatial resolution. Direct observation of plasma inhomogeneity effects has been enabled.

The integration of artificial intelligence and autonomous spectroscopy marks a paradigm shift from passive measurement to active, intelligent experimentation. Physics-informed neural networks (PINNs) that combine conservation laws with deep learning architectures have shown promise for real-time spectral deconvolution. Separation of overlapping broadening contributions has been achieved with uncertainties below 1% even in highly non-equilibrium plasmas. AI-driven systems also enable adaptive spectroscopy. In these systems, experimental parameters such as pressure, delay time, and laser power are dynamically optimized in real time to achieve optimal resolution for specific analytes. These capabilities are transformative for complex multi-element analyses. Traditional fixed-parameter approaches often fail to achieve adequate resolution across diverse atomic transitions.

Novel broadening suppression strategies are emerging that challenge conventional low-pressure operation. Active compensation using acousto-optic or electro-optic modulators permits real-time correction of Doppler shifts in turbulent plasmas. Cryogenic plasma jet techniques have demonstrated translational temperatures below 50 K in atmospheric pressure environments. Coherent control methods borrowed from quantum optics enable selective excitation of specific velocity groups within the Maxwell–Boltzmann distribution. Doppler broadening can thus be effectively eliminated without the signal loss associated with sub-Doppler techniques.

These technological advances converge to enable applications once relegated to theoretical speculation. Single-atom isotope detection is now feasible through the combination of laser cooling, quantum state manipulation, and ultrahigh-resolution spectroscopy. *In situ* nuclear reactor monitoring using radiation-hardened LAAS systems promises real-time isotopic analysis in extreme radiation environments, crucial for next-generation safety protocols. Precision spectroscopy at atmospheric pressure is no longer constrained by low-pressure paradigms. Advanced deconvolution algorithms and ultra-narrow linewidth sources enable field-deployable systems for environmental monitoring and nuclear nonproliferation.

The maturation of LAAS as a quantitative analytical technique necessitates the development of rigorous standardization and metrology frameworks. International spectroscopic standards must incorporate certified reference materials and standardized protocols for broadening parameter measurements across all elements. Uncertainty quantification frameworks that account for the interplay of broadening mechanisms, instrumental effects, and environmental factors must be established. Such frameworks will enable LAAS certification for critical applications in nuclear forensics and medical diagnostics.

Looking forward, the synergistic combination of these developments points toward a future where LAAS achieves theoretical resolution limits while maintaining practical applicability across diverse fields. The next decade is expected to witness the emergence of LAAS as the definitive technique for ultrahigh-resolution atomic spectroscopy. Capabilities will extend from single-atom sensitivity to real-time process monitoring in extreme environments. As instrumental broadening approaches zero and computational methods enable perfect deconvolution of physical broadening mechanisms, the ultimate limits of LAAS will be determined by the fundamental quantum mechanical properties of matter.

6. Conclusions

This review provides an overview of the current principles of spectral broadening and their implications for LAAS. As a significant analytical technique, LAAS plays a crucial role in various fields, including nuclear forensics, chemical detection, medical diagnostics, environmental monitoring, and numerous industrial applications. To improve the accuracy of LAAS, it is essential to account for broadening effects, particularly the more impactful mechanisms such as Stark, Doppler, and pressure broadening. Spectral broadening directly impacts the resolution, sensitivity, and accuracy of LAAS by altering the shape and width of spectral lines, which are critical for quantifying analytes in complex matrices.

Stark broadening, induced by external electric fields, is critical for plasma diagnostics and electron density determination, making it a priority in environments with strong electric fields. Doppler broadening, influenced by the thermal motion of atoms or molecules, must be carefully considered when assessing gas temperatures, especially in high-temperature environments where its effects are most pronounced. Pressure broadening, caused by particle interactions within the plasma, is significant under elevated pressure conditions and must be considered in applications such as isotope analysis and gas sensing.

In comparison, the contributions of natural and instrumental broadening to LAAS are generally minor and can be disregarded in most routine applications. However, in high-precision scenarios, even these small effects may require careful correction. Looking forward, LAAS is approaching a critical stage of development. The integration of several emerging technologies, including artificial intelligence for spectral analysis, non-LTE theoretical modeling, and ultrafast time-resolved diagnostics, is expected to overcome many of the technique's longstanding limitations. Further improvements in measurement methodology and plasma modeling are anticipated to increase the accuracy and robustness of LAAS. These advances will expand its application scope, particularly in isotope ratio determination, plasma diagnostics under non-equilibrium conditions, and precision measurements in extreme environments.

Data availability

This review is based on data and findings from previously published studies. No new datasets were generated or analyzed. All data sources are cited in the references section of this article.

Author contributions

Erfan Chenshen: conceptualization; Juntao Tan: conceptualization, copyright acquisition of the figures; Bin Wang, Erlong Jiang, Shaofeng Zheng, Zeren Luo: collection and analysis of the literature; Nan Zhao, Jiaming Li: funding acquisition; supervision; project administration; writing – review and editing; Qingmao Zhang: resources. All the authors discussed the structure of the manuscript and commented on the manuscript.

Conflicts of interest

All authors disclosed no relevant relationships.

Acknowledgements

This work was supported by the National Natural Science Foundation of China (62475075); Guangdong Basic and Applied Basic Research Foundation (2023A1515011641, 2023A1111120030); Young Talent Support Project of Guangzhou Association for Science and Technology (QT-2023-007); The Open Project of Guangdong Provincial Key Laboratory of Intelligent Port Security Inspection (2023B1212010011).

Notes and references

1 B. Welz, H. Becker-Ross, S. Florek and U. Heitmann, *High-Resolution Continuum Source AAS: the Better Way to Do Atomic Absorption Spectrometry*, 2005.
2 B. Kartoğlu, S. Bodur, D. Zeydanlı, T. Göver, E. Özaydın, E. Gülhan Bakırdere and S. Bakırdere, *Food Chem.*, 2024, **439**, 138140.
3 J. Chen and K. C. Teo, *Anal. Chim. Acta*, 2001, **450**, 215–222.
4 Y. Kilinç, B. T. Zaman, S. Bakirdere and N. Özdoğan, *Food Chem.*, 2024, **432**, 137244.
5 M. J. Cal-Prieto, M. Felipe-Sotelo, A. Carlosena, J. M. Andrade, P. López-Mahía, S. Muniategui and D. Prada, *Talanta*, 2002, **56**, 1–51.
6 M. Y. Burylin and A. A. Pupyshev, *J. Anal. Chem.*, 2017, **72**, 935–946.
7 D. J. Butcher, *Appl. Spectrosc. Rev.*, 2024, **59**, 247–275.
8 D. J. Butcher, *Appl. Spectrosc. Rev.*, 2023, **58**, 65–82.
9 N. Pourreza and K. Ghanemi, *J. Hazard. Mater.*, 2010, **178**, 566–571.
10 S. Bodur, S. Erarpat, İ. Kayın and S. Bakırdere, *Chem. Pap.*, 2023, **77**, 6629–6636.
11 N. H. Bings, A. Bogaerts and J. A. C. Broekaert, *Anal. Chem.*, 2010, **82**, 4653–4681.
12 P. Sangwan, C. Nimi, T. Nain, N. Sharma and R. Singh, *Indian J. Sci. Technol.*, 2024, **17**, 1087–1096.
13 W. J. Price, *Annu. Rep. Anal. Atomic Spectrosc.*, 1980, **10**, 1–30.
14 F. Zaccheria, N. Ravasio, R. Psaro and A. Fusi, *Chem.–Eur. J.*, 2006, **12**, 6426–6431.
15 D. L. Tsalev, *Spectrochim. Acta, Part B*, 2000, **55**, 917–933.
16 G. Hull, E. D. McNaghten, C. A. Sharrad and P. A. Martin, *Spectrochim. Acta, Part B*, 2022, **190**, 106378.
17 M. Burger, P. J. Skrodzki, I. Jovanovic, M. C. Phillips and S. S. Harilal, *Phys. Plasmas*, 2019, **26**, 093103.
18 E. H. Kwapis, J. Borrero, K. S. Latty, H. B. Andrews, S. S. Phongikaroon and K. C. Hartig, *Appl. Spectrosc.*, 2023, **78**, 9–55.
19 J. Li, Z. Yu, Z. Du, Y. Ji and C. Liu, *Remote Sens.*, 2020, **12**(17), 2771.
20 G. Hull, E. D. McNaghten, P. Coffey and P. Martin, *Spectrochim. Acta, Part B*, 2021, **177**, 106051.
21 W. Chen, S. Qiao, Z. Zhao, S. Gao, Y. Wang and Y. Ma, *Microwave Opt. Technol. Lett.*, 2024, **66**, e33780.
22 C. M. Murzyn, D. J. Allen, A. N. Baca, A. A. Egeln, R. W. Houim, D. R. Guildenbecher, R. T. Marinis and M. C. Welliver, *J. Appl. Phys.*, 2024, **135**, 013101.

23 T. Stacewicz, Z. Bielecki, J. Wojtas, P. Magryta, J. Mikolajczyk and D. Szabra, *Opto-Electron. Rev.*, 2016, **24**, 82–94.

24 P. J. Parsons and F. Barbosa, *Spectrochim. Acta, Part B*, 2007, **62**, 992–1003.

25 Z. Zhou, C. Shen, W. Long, J. Chen, J. Lu, L. Gao, Y. Hu, M. Yu, X. Wu and J. Shao, *Spectrochim. Acta, Part A*, 2024, **308**, 123750.

26 B. Fu, C. Zhang, W. Lyu, J. Sun, C. Shang, Y. Cheng and L. Xu, *Appl. Spectrosc. Rev.*, 2022, **57**, 112–152.

27 C. L. Schiller, S. Locquiao, T. J. Johnson and G. W. Harris, *J. Atmos. Chem.*, 2001, **40**, 275–293.

28 A. Elkhazraji, M. Sy, M. Mhanna, J. Aldhawyan, M. Khaled Shakfa and A. Farooq, *Exp. Therm. Fluid Sci.*, 2024, **151**, 111090.

29 J. Xia, Y. Xia, D. Xiao, R. Zhang, N. Yu and C. Liu, *Sens. Actuators, B*, 2024, **418**, 136258.

30 P. zhao, D. Ding, K. Li, Y. Li and G. Jin, *Opt. Commun.*, 2024, **567**, 130327.

31 J. Lu, C. Shen, Z. Zhou, Y. Zhang, J. Wang, Y. Liang, J. Wang, J. Lu, C. Fan, X. Dong and J. Shao, *Opt. Lasers Eng.*, 2024, **173**, 107899.

32 M. Lackner, *Rev. Chem. Eng.*, 2007, **23**, 65–147.

33 S. Carter, A. S. Fisher, P. S. Goodall, M. W. Hinds, S. Lancaster and S. Shore, *J. Anal. At. Spectrom.*, 2011, **26**, 2319–2372.

34 H. R. Griem, Plasma spectroscopy, *Science*, 1964, **147**, 284.

35 H. R. Griem, Spectral line broadening by plasmas, *Pure Appl. Phys.*, 1974, **39**, 0079–8193.

36 C. Penache, M. Miclea, A. Bräuning-Demian, O. Hohn, S. Schössler, T. Jahnke, K. Niemax and H. Schmidt-Böcking, *Plasma Sources Sci. Technol.*, 2002, **11**, 476.

37 S. S. Harilal, B. E. Brumfield, N. L. LaHaye, K. C. Hartig and M. C. Phillips, *Appl. Phys. Rev.*, 2018, **5**, 021301.

38 M. Miyabe, M. Oba, H. Iimura, K. Akaoka, Y. Maruyama, H. Ohba, M. Tampo and I. Wakaida, *Hyperfine Interact.*, 2013, **216**, 71–77.

39 A. Kuwahara, Y. Aiba, T. Nankawa and M. Matsui, *J. Anal. At. Spectrom.*, 2018, **33**, 893–896.

40 A. Kuwahara, Y. Aiba, S. Yamasaki, T. Nankawa and M. Matsui, *J. Anal. At. Spectrom.*, 2018, **33**, 1150–1153.

41 P. Jacquet and A. Pailloux, *J. Anal. At. Spectrom.*, 2013, **28**, 1298–1302.

42 V. Lebedev, J. H. Bartlett and A. Castro, *J. Anal. At. Spectrom.*, 2018, **33**, 1862–1866.

43 G. Qi, Y.-B. Huang, J. Huang, X.-J. Lu, T. Yang and Z.-S. Cao, *J. Anal. At. Spectrom.*, 2024, **39**, 935–941.

44 S. S. M. Hassan, *Organic Analysis Using Atomic Absorption Spectrometry*, 1984.

45 D. A. Cremers and L. J. Radziemski, *Handbook of Laser-Induced Breakdown Spectroscopy*, John Wiley & Sons, 2013.

46 A. M. El Sherbini, A. M. Aboulfotouh, S. H. Allam and T. M. El Sherbini, *Spectrochim. Acta, Part B*, 2010, **65**, 1041–1046.

47 N. Sadeghi, *J. Quant. Spectrosc. Radiat. Trans.*, 2024, **315**, 108868.

48 N. Konjević, M. Ivković and N. Sakan, *Spectrochim. Acta, Part B*, 2012, **76**, 16–26.

49 D. M. Surmick and C. G. Parigger, *Int. Rev. At. Mol. Phys.*, 2014, **5**, 73–81.

50 I. B. Gornushkin, L. A. King, B. W. Smith, N. Omenetto and J. D. Winefordner, *Spectrochim. Acta, Part B*, 1999, **54**, 1207–1217.

51 M. S. Dimitrijević, *Data*, 2020, **5**, 73.

52 R. J. Peláez, S. Djurović, M. Ćirišan, J. A. Aparicio and S. Mar, *Astron. Astrophys.*, 2012, **539**, A40.

53 J. Purić, I. P. Dojčinović, M. Nikolić, M. Šćepanović, B. M. Obradović and M. M. Kuraica, *Astrophys. J.*, 2008, **680**, 803.

54 R. J. Peláez, S. Djurović, M. Ćirišan, J. A. Aparicio and S. Mar, *Astron. Astrophys.*, 2010, **518**, A60.

55 J. Purić and M. Šcepanović, *Astrophys. J.*, 1999, **521**, 490.

56 H. Liu, B. S. Truscott and M. N. R. Ashfold, *Plasma Sources Sci. Technol.*, 2016, **25**, 015006.

57 J. Thouin, M. Benmouffok, P. Freton and J.-J. Gonzalez, *Eur. Phys. J. Appl. Phys.*, 2022, **97**, 87.

58 S. S. Harilal, E. J. Kautz and M. C. Phillips, *Phys. Rev. E*, 2021, **103**, 013213.

59 N. L. LaHaye, S. S. Harilal and M. C. Phillips, *Spectrochim. Acta, Part B*, 2021, **179**, 106096.

60 V. Radhakrishna, R. J. Tancin and C. S. Goldenstein, *Appl. Phys. Lett.*, 2022, **121**, 031105.

61 A. Quentmeier, M. Bolshov and K. Niemax, *Spectrochim. Acta, Part B*, 2001, **56**, 45–55.

62 S. S. Harilal, C. M. Murzyn, M. C. Phillips and J. B. Martin, *Spectrochim. Acta, Part B*, 2020, **169**, 105828.

63 S. S. Harilal, E. J. Kautz, R. J. Jones and M. C. Phillips, *Plasma Sources Sci. Technol.*, 2021, **30**, 045007.

64 N. Q. Minesi, A. P. Nair, M. O. Richmond, N. M. Kuenning, C. C. Jelloian and R. M. Spearrin, *Appl. Opt.*, 2023, **62**, 782–791.

65 N. Konjević, A. Lesage, J. R. Fuhr and W. L. Wiese, *J. Phys. Chem. Ref. Data*, 2002, **31**, 819–927.

66 I. I. Sobelman, *Atomic Spectra and Radiative Transitions*, Springer Science & Business Media, 2012.

67 H. Liu, A. Quentmeier and K. Niemax, *Spectrochim. Acta, Part B*, 2002, **57**, 1611–1623.

68 E. J. Kautz, A. Xu, A. V. Harilal, M. P. Polek, A. M. Casella, D. J. Senor and S. S. Harilal, *Opt. Express*, 2023, **31**, 3549–3564.

69 N. Konjević, *Phys. Rep.*, 1999, **316**, 339–401.

70 P. Kumar, S. Soumyashree, N. Rao Epuru, S. B. Banerjee, R. P. Singh and K. P. Subramanian, *Appl. Spectrosc.*, 2020, **74**, 913–920.

71 M. Miyabe, M. Oba, H. Iimura, K. Akaoka, Y. Maruyama, I. Wakaida and K. Watanabe, *AIP Conf. Proc.*, 2009, **1104**, 30–35.

72 M. Miyabe, M. Oba, H. Iimura, K. Akaoka, Y. Maruyama and I. Wakaida, *Appl. Phys. A*, 2010, **101**, 65–70.

73 M. Miyabe, M. Oba, H. Iimura, K. Akaoka, A. Khumaeni, M. Kato and I. Wakaida, *Spectrochim. Acta, Part B*, 2015, **110**, 101–117.

74 M. Miyabe, M. Oba, K. Jung, H. Iimura, K. Akaoka, M. Kato, H. Otobe, A. Khumaeni and I. Wakaida, *Spectrochim. Acta, Part B*, 2017, **134**, 42–51.

75 C. Aragón and J. A. Aguilera, *Spectrochim. Acta, Part B*, 2008, **63**, 893–916.

76 R. G. Wala, M. C. Phillips, S. S. Harilal, R. J. Jones and M. P. Polek, *Spectrochim. Acta, Part B*, 2024, **10**, 7142.

77 B. A. Bushaw and N. C. Anheier, *Spectrochim. Acta, Part B*, 2009, **64**, 1259–1265.

78 A. Kuwahara, K. Murakami, H. Tomita, K. Sawada and Y. Enokida, *J. Anal. At. Spectrom.*, 2022, **37**, 2033–2041.

79 A. e. Farsy, V. G. Antunes, B. Seznec, L. Schiesko, C. Ballage and T. Minea, *J. Appl. Phys.*, 2022, **132**, 054904.

80 M. C. Phillips, E. J. Kautz and S. S. Harilal, *Opt. Lett.*, 2023, **48**, 1942–1945.

81 H. D. Wizemann and K. Niemax, *Anal. Chem.*, 1997, **69**, 4291–4293.

82 S. Nishiyama, K. Takada and K. Sasaki, *Jpn. J. Appl. Phys.*, 2021, **60**, 076001.

83 L. A. King, I. B. Gornushkin, D. Pappas, B. W. Smith and J. D. Winefordner, *Spectrochim. Acta, Part B*, 1999, **54**, 1771–1781.

84 M. P. Polek, M. C. Phillips, F. N. Beg and S. S. Harilal, *Spectrochim. Acta, Part B*, 2025, **229**, 107191.

85 B. W. Smith, A. Quentmeier, M. Bolshov and K. Niemax, *Spectrochim. Acta, Part B*, 1999, **54**, 943–958.

86 B. A. Bushaw and M. L. Alexander, *Appl. Surf. Sci.*, 1998, **127–129**, 935–940.

87 D. A. Cremers, A. Beddingfield, R. Smithwick, R. C. Chinni, C. R. Jones, B. Beardsley and L. Karch, *Appl. Spectrosc.*, 2012, **66**, 250–261.

88 K. C. Hartig, PhD thesis, PennState University, 2016, p. 191.

89 C. A. Smith, M. A. Martinez, D. K. Veirs and D. A. Cremers, *Spectrochim. Acta, Part B*, 2002, **57**, 929–937.

90 N. R. Taylor and M. C. Phillips, *Opt. Lett.*, 2014, **39**, 594–597.

91 W. Wei, I. Savukov and A. Castro, *J. Anal. At. Spectrom.*, 2021, **36**, 1912–1920.

92 H. R. Griem, *Principles of Plasma Spectroscopy*, 2005.

93 H. J. Kunze, *Introduction to Plasma Spectroscopy*, Springer Science & Business Media, 2009, p. 242.

94 T. N. Anderson, J. K. Magnuson and R. P. Lucht, *Appl. Phys. B*, 2007, **87**, 341–353.

95 T. R. Adowski and P. T. Bauman, *J. Thermophys. Heat Transfer*, 2019, **33**, 738–748.

96 Z. Wang, *Chemosensors*, 2025, **13**(1), 5.

97 C. Schnürer-Patschan, A. Zybin, H. Groll and K. Niemax, *J. Anal. At. Spectrom.*, 1993, **8**, 1103–1107.

98 H. D. Wizemann and K. Niemax, *Spectrochim. Acta, Part B*, 2000, **55**, 637–650.

99 H. D. Wizemann, *Spectrochim. Acta, Part B*, 1999, **54**, 1267–1278.

100 H.-D. Wizemann, *J. Anal. At. Spectrom.*, 2000, **15**, 1401–1403.

101 H. D. Wizemann and U. Haas, *Spectrochim. Acta, Part B*, 2003, **58**, 931–947.

102 G. A. Mark, *Meas. Sci. Technol.*, 1998, **9**, 545.

103 R. J. Lipert, *Appl. Spectrosc.*, 1998, **52**, 1172–1178.

104 I. Draganić, J. R. Crespo López-Urrutia, R. DuBois, S. Fritzsche, V. M. Shabaev, R. S. Orts, I. I. Tupitsyn, Y. Zou and J. Ullrich, *Phys. Rev. Lett.*, 2003, **91**, 183001.

105 C. Wu, C. Dong and X. Ding, *Phys. Lett. A*, 2024, **522**, 129805.

106 A. D. Ludlow, M. M. Boyd, J. Ye, E. Peik and P. O. Schmidt, *Rev. Mod. Phys.*, 2015, **87**, 637–701.

107 Y. Wu, F. Qin, Z. Ding, R. Xu and D. Li, *Photonics*, 2024, **11**(4), 298.

108 N. Liu, T. Y. Chen, H. Zhong, Y. Lin, Z. Wang and Y. Ju, *Appl. Phys. Lett.*, 2022, **120**, 201103.

109 J. Bergevin, T.-H. Wu, J. Yeak, B. E. Brumfield, S. S. Harilal, M. C. Phillips and R. J. Jones, *Nat. Commun.*, 2018, **9**, 1273.

110 F. Bredice, F. O. Borges, H. Sobral, M. Villagran-Muniz, H. O. Di Rocco, G. Cristoforetti, S. Legnaioli, V. Palleschi, L. Pardini, A. Salvetti and E. Tognoni, *Spectrochim. Acta, Part B*, 2006, **61**, 1294–1303.